

Direct Ink Writing of Recycled Composites with Complex Shapes: Process Parameters and Ink Optimization

Andrea Mantelli, Alessia Romani, Raffaella Suriano,* Marinella Levi, and Stefano Turri

Within the complex framework of additive manufacturing, direct ink writing (DIW) processes significantly contribute to extending the range of 3D-printable materials (i.e., thermosetting resins, ceramics, hydrogels). Thanks to this technology, viscous inks are easily extruded for the creation of 3D structures. Nevertheless, the quick recovery of the solid-like behavior after extrusion remains one of the most crucial open issues for 3D-printable inks. The main goal herein is to improve the printability of a UV-curable thermosetting composite ink reinforced with mechanically recycled glass fiber composites by modifying its rheological behavior. The overall process is optimized, leading to the definition of the optimal extrusion parameters for these types of materials. Furthermore, the retraction mode is successfully developed for the DIW of recycled composites. Additional features are achieved, thanks to the aforementioned improvements, such as 3D complex shapes, assembled pieces, and/or moving built-in mechanisms, increasing the number of new potential applications of recycled glass fiber-reinforced polymers.

The DIW technology allows the 3D printing of various inks such as hydrogels for biomedical applications,^[8,9] ceramic materials, ionogels, and nanocomposites for sensors and energy devices.^[10–12] However, one of the main challenges of DIW printing is to design and formulate printable inks that flow like a liquid under shear and quickly recover a solid-like behavior just after extrusion through the printing nozzle. In recent years, many approaches have been adopted to face this challenge and develop inks composed of a wide range of materials for DIW. Soft elastomeric structures composed of particle-free silicone oil-in-water emulsions with high extensional strain to break were 3D printed, thanks to the addition of a polymer additive, poly(ethylene oxide), which increased the material stability during extrusion.^[13] Regarding the 3D printing

1. Introduction


Additive manufacturing (AM) technologies have completely transformed the traditional processes of product design and fabrication, offering more flexibility in the design process and the possibility of prototyping or building complicated structures with customized geometry.^[1,2] Moreover, a wide choice of materials ranging from thermoplastics to metals, from ceramic materials to reinforced polymers, can be processed using different types of AM technologies,^[3,4] such as fused deposition modeling (FDM),^[5] selective laser sintering, and stereolithography.^[6] Among them, direct ink writing (DIW) enables the extrusion of viscous inks instead of solid filaments, usually melted in an FDM 3D printer.^[7]

of stiff structures, the definition of a dimensionless number, combining the importance of both gravitational slumping and capillary forces in printed ceramic materials, led to good shape fidelity of printed ceramic objects with high density and flexural strength compared with commercial ceramics.^[14] Even borosilicate glass-based objects, which usually have low shape retention after the printing and sintering process, were successfully 3D printed, thanks to the dispersion of the glass powder in a polymer hydrogel, which allowed the fast recovery of a gel-like behavior after being sheared at high deformations. This was observed by thixotropic rheological tests and it appeared to be of paramount importance to ensure the shape retention of materials at low deformation stresses after extrusion.^[15] Similar rheological tests were conducted to optimize the printability of cementitious composites.^[16]

The addition of plasticizers, as well as viscosity-modifying agents and rheological modifiers, has been a strategy validated for Portland cement-based concretes to simultaneously provide the flowability and shape retention to the extruded elements.^[17] A rheological modifier was also the approach developed by Sun et al. to create a hydrogen-bond network in a UV-curable acrylate/epoxy resin, thus inducing a yield stress behavior after extrusion in this low-viscous cross-linkable system.^[18]

In this work, a rheology additive with antisagging effects was added to a UV- and thermocurable acrylate ink filled with mechanically recycled glass fiber-reinforced polymers (rGFRPs), aiming at generating a 3D network structure in this 3D-printable system. The resulting flow behavior of this UV-

A. Mantelli, A. Romani, Dr. R. Suriano, Prof. M. Levi, Prof. S. Turri
Department of Chemistry, Materials and Chemical Engineering “Giulio Natta”
Politecnico di Milano
Piazza Leonardo da Vinci 32, Milano 20133, Italy
E-mail: raffaella.suriano@polimi.it

 The ORCID identification number(s) for the author(s) of this article can be found under <https://doi.org/10.1002/adem.202100116>.

© 2021 The Authors. Advanced Engineering Materials published by Wiley-VCH GmbH. This is an open access article under the terms of the Creative Commons Attribution License, which permits use, distribution and reproduction in any medium, provided the original work is properly cited.

DOI: 10.1002/adem.202100116

curable ink rheologically modified and reinforced with rGFRPs enabled the control of the flowability and printing resolution during a UV-assisted DIW process. Recently, some studies presented the 3D printing of thermoplastic polymers reinforced with end-of-life (EoL) products^[19] and production wastes^[20] by FDM. However, to the best of our knowledge, there are no examples of scientific works, showing the relationship between the rheological behavior and the printability of UV-curable systems reinforced with rGFRPs by DIW. Mechanically recycled composite materials are typically characterized by batch variability, due to differences between EoL products obtained by diverse manufacturers, and by intrinsically heterogeneous material composition, due to the presence of matrix particles and reinforcing fillers. Consequently, different results between batches can be obtained during the 3D printing DIW process, and they cannot be properly predicted by applying the existing knowledge that relates the rheological behavior to the printability of UV-curable systems reinforced with virgin conventional fillers.

To overcome this issue and find the optimal parameters for rGFRPs ink formulation and the DIW process, a specific methodology, consisting of rheological and printing tests, was designed and developed in this work for the first time. For this reason, the goal of this work is to demonstrate the printability control of a cross-linkable acrylate resin reinforced with rGFRPs through the study of the ink rheological properties. This led to an optimization of the UV-assisted DIW process already developed in a previous work, presenting the 3D printing of UV- and thermocurable resins loaded with mechanically rGFRPs obtained by shredding EoL wind blades.^[21] Moreover, a better understanding of the optimal extrusion parameters for composites reinforced with rGFRPs, based on rheological analysis and print tests, led to the development of the retraction mode for the DIW fabrication technique. While the retraction mode is a base feature for FDM, it can be very challenging for DIW processes. This study, therefore, opens new opportunities for the AM of complex structures, supporting at the same time the future of new developments and applications of circular economy models for GFRPs.

2. Results and Discussion

2.1. Extrusion Model

The relation between process parameters and material viscosity has been extensively discussed in the literature. Many works define printability as the capability of the material to self-sustain after the extrusion process and maintain the fabricated shape.^[14,22,23] Others relate the extrusion force produced by an FDM extruder to the rheological properties of a molten polymer.^[24,25] The models already available in literature do not consider differences in rheological behavior during the extrusion process of a 3D-printable ink. In a previous work, rGFRP inks showed a Newtonian behavior at lower shear rates and a pseudoplastic behavior at higher shear rates.^[26] By considering these differences and focusing on the DIW of rGFRPs inks, the model proposed in this work will be used to better estimate their extrudability, which can be defined as their ability to be properly

extruded in a DIW extruder. This will allow a better understanding of some parameters, which affect the first step of the 3D printing process.

2.1.1. Extruder Maximum Pressure

The extruder assembly, which is shown in Figure S1, Supporting Information, is composed of a gear train powered by a stepper motor, a lead screw, and a syringe.^[27] Known the maximum torque of the stepper motor and the parameters of the gears, the maximum pressure developed by the extruder is 1.8 MPa, as shown in Note N1, Supporting Information.

2.1.2. Maximum Viscosity Model

For a general pseudoplastic material, which complies with the power-law model,^[28] the flow consistency (k) and the flow behavior index (n) define the rheological behavior, as follows

$$\eta = k \cdot \dot{\gamma}^{n-1} \quad (1)$$

Comparing the maximum pressure generated by the extruder and the pressure drop inside the extrusion path, k and the viscosity (η) can be, respectively, calculated as a function of the volumetric flow and the shear rate ($\dot{\gamma}$) according to the following equations (please refer to Note N2, Supporting Information, for the complete derivation)

$$k < \frac{c_i \cdot P_0 \cdot d_i}{4l_i} \left(\frac{\pi \cdot d_i^3 \cdot n_i}{8 \cdot Q \cdot (3n_i + 1)} \right)^{n_i} \quad (2)$$

$$\eta < \frac{c_i \cdot P_0 \cdot d_i}{4l_i \cdot \dot{\gamma}_i} \quad (3)$$

where c_i is the ratio between the pressure drop inside the segment i of the extrusion path and the total pressure drop, P_0 is the maximum pressure generated by the extruder, d_i and l_i are, respectively, the diameter and the length of the segment i of the extrusion path, and Q is the volumetric flow rate. As described in the Note N2, Supporting Information, when the rheological behavior of the ink changes during the extrusion process, n_i , the flow behavior index in segment i is a function of Q , and the shear rate in segment i is a function of Q and n_i .

$$\dot{\gamma}_i = \frac{8Q}{\pi d_i^3} \left[\frac{3n_i + 1}{n_i} \right] \quad (4)$$

2.1.3. Linking the Viscosity Model with the Extrusion Process

The maximum k value, expressed by Equation (2), was calculated for different process parameters to better understand the link between the model and the extrusion process. Three materials were considered: 1) a Newtonian ink; 2) a pseudoplastic ink with n equal to 0.5; and 3) a pseudoplastic ink with $n = 0.1$. Calculations were carried out considering a 20 mL syringe equipped with three different dispensing tips: 1) a conical metal tip; 2) a conical plastic tip; and 3) a cylindrical metal tip; herein-after called MT18G, TT18G, and TE18G, respectively. Finally, three different layer heights and five print velocities were

considered for the calculations. The volumetric flow rate was calculated with Equation (5) considering a constant print line width equal to 1 mm for all the dispensing tips

$$Q = w \cdot h \cdot v_p \quad (5)$$

where w is the print line width, h the layer height, and v_p the print velocity.

Figure 1 shows the results of the calculations. In general, pseudoplastic inks are to be preferred, considering that the maximum k value has a lower variability than Newtonian inks in a wide range of process parameters (e.g., printing speed, layer height). Considering the different geometries of the dispensing tips, both MT18G and TE18G provide a pressure drop lower than TT18G with pseudoplastic inks (Figure 1b). This result can be due to the lower length of the MT18G and TE18G tips compared with that of TT18G.

As shown in Figure 1a, the TE18G tip has the same performance as MT18G for the pseudoplastic ink with n equal to 0.1. Despite this, the MT18G tip was selected in this work because it provides the higher k values for all the inks.

2.2. Rheological Analysis

The rheological behavior of different rGFRP inks was tested to verify the validity of the described model and better understand the behavior of acrylate resin reinforced with rGFRP. As a further step in the development of the recycled composite ink, an anti-sagging additive, hereinafter called BYK, was added to the formulation to foster the ink's self-standing ability and thus improve ink printability, which depends not only on the extrudability but also, for instance, on the shape retention and the solid-like behavior recovery after the extrusion.

Two sets of inks based on acrylate resin were studied. The first set is composed of three inks filled with 50, 55, and 60 wt% of mechanically rGFRPs. The second set is composed of three inks with a fixed content of the rGFRP (55 wt%) and an increasing amount of the BYK additive (3, 6, 9 wt%). In the following, the different inks will be named XBYR, where X is the wt%

of the BYK additive and Y is the wt% of rGFRP. An additional ink which is filled with 55 wt% of virgin glass fibers is used as a reference sample, named 0B55V.

2.2.1. Extrudability

Flow ramp tests were conducted either without a preshear step or by applying preshear. The preshear step was meant to simulate the material loading into the syringe. On the contrary, without applying preshear, it was possible to measure the difference in viscosity of the material in the syringe after a period of rest from loading.

As shown in **Figure 2**, the effect of preshear is significant. Considering the first set of inks (Figure 2a,b), the effect of preshear is negligible for 0B50R ink and increases by increasing the rGFRP content. The addition of the BYK additive mitigated the viscosity reduction due to the preshear. As shown in Figure 2c,d, the viscosity of the second set of inks after preshear is lower than the viscosity measured without preshear. Nevertheless, the difference is lower compared with 0B55R viscosity with and without preshear (Figure 2a,b). To sum up, an increase in the viscosity was observed by increasing the rGFRP content. On the contrary, the BYK additive content has no significant effect on the viscosity behavior.

Extrapolating the power-law model parameters (Equation (1)) from the experimental curves, it is possible to calculate the maximum allowed viscosity for the different inks. **Table 1** shows the k and n values extrapolated from all the viscosity curves of the inks.

Except for 0B60R ink, all other inks show two different power-law behaviors. It was observed that the inks have a higher n value at lower shear rates compared with higher shear rates. Considering the bigger cross section of the syringe reservoir than the exit segment, the material was subjected to lower shear rates in the first segment and higher ones in the last segment of the dispensing tip. Therefore, the maximum viscosity for the ink in the syringe reservoir and at the exit zone can be calculated using Equation (3) and the different n values shown in Table 1. As shown in Figure 2, the maximum viscosity is higher than the

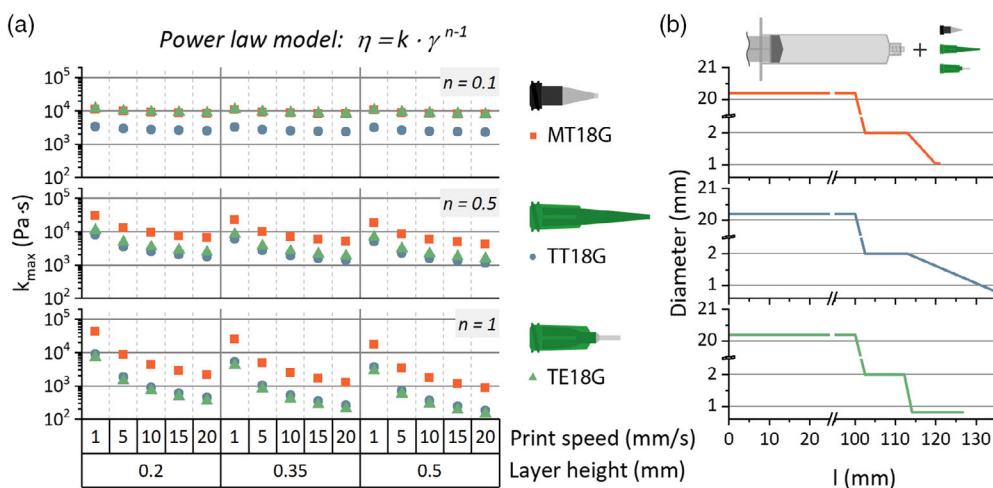


Figure 1. Maximum viscosity model results as a function of the print parameters, dispensing tips geometry, and the flow behavior index (n): a) maximum flow consistency index (k_{max}) and b) extrusion path diameters for the three dispensing tips geometry as a function of the length of the extrusion path l .

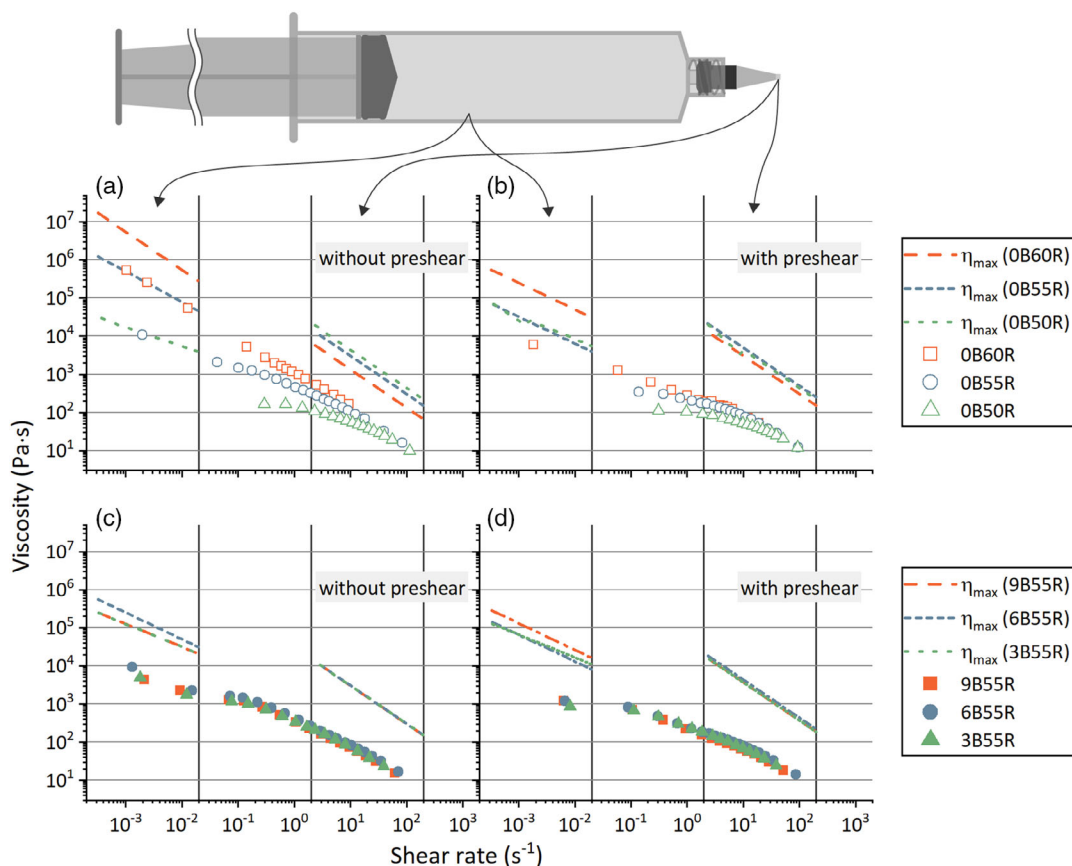


Figure 2. Log–log plots of viscosity as a function of shear rate and max viscosity evaluated with the analytical model: flow ramp tests conducted on inks without the rheological modifier and different wt% of recyclate: a) without the preshear step and b) with the preshear step; flow ramp tests conducted on inks with different wt% of rheological modifier and 55 wt% of recyclate: c) without the preshear step and d) with the preshear step. The max viscosity was evaluated at a lower shear rate for the material inside the syringe and a higher shear rate for the material in the exit segment of the dispensing tip by extrapolating the flow behavior index from the experimental curves (Table 1).

Table 1. Flow behavior index (n), flow consistency index (k), and the onset of the behavior change extrapolated from flow ramp experimental curves.

Ink	Without preshear step					With preshear step				
	n_1	k_1 [Pa·s]	Onset [s^{-1}]	n_2	k_2 [Pa·s]	n_1	k_1 [Pa·s]	Onset [s^{-1}]	n_2	k_2 [Pa·s]
OB50R	1.0	166	0.6	0.5	168	0.9	103	1.6	0.5	140
OB55R	0.5	487	0.2	0.3	477	0.9	317	0.2	0.6	222
OB55V	1.0	227	0.5	0.4	147	1.0	95	0.5	0.7	75
OB60R	0.1	1097	n.d.	n.d.	n.d.	0.6	249	0.04	0.3	131
3B55R	0.7	444	0.1	0.3	334	0.8	356	0.1	0.4	244
6B55R	0.6	437	0.1	0.3	403	0.8	399	0.1	0.5	260
9B55R	0.7	509	0.1	0.3	335	0.7	303	0.1	0.4	220

viscosity of the ink in all the shear rate ranges considered. This result can be also confirmed by comparing the k values extrapolated from the viscosity curves (Table 1) with the maximum k values shown in Figure 1a. This indicates that the inks investigated in this work never showed a viscosity higher than the maximum value defined by the maximum viscosity model, confirming the extrudability of these types of inks. Table 1 also shows that the k and n values for OB55V ink are very similar to

OB50R values. This suggests that the extrudability and viscosity behavior of inks loaded with virgin glass fibers are comparable with those filled with mechanically rGFRPs. However, the latter ones are to be preferred from an environmental point of view, enabling sustainable recycling of EoL wind blades in their decommissioning phase of life. For this reason, rGFRPs were used in this study and were chosen as fillers in place of virgin glass fibers.

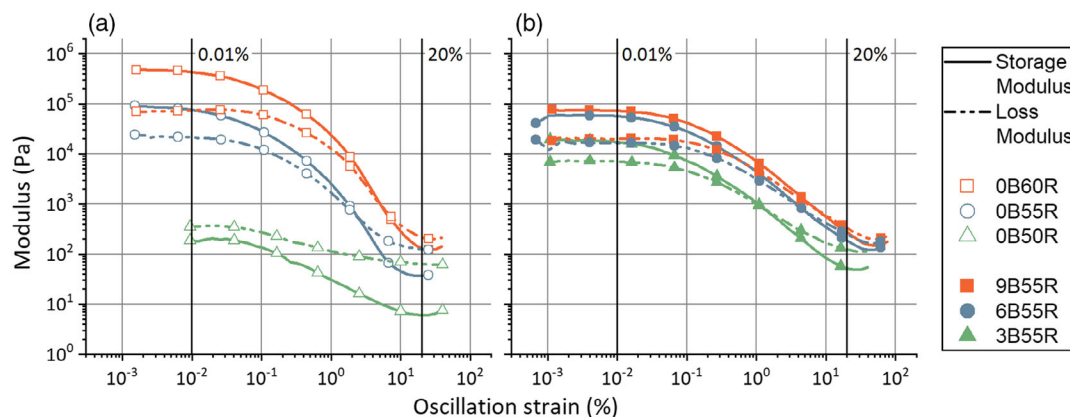


Figure 3. Log–log plots of the storage and loss modulus as a function of the oscillation strain: strain sweep test conducted at 1 Hz on a) inks without the rheological modifier and different wt% of recyclate and b) inks with different wt% of the rheological modifier and 55 wt% of the recyclate.

2.2.2. Self-Standing Ability

To study the self-standing ability, oscillatory tests were conducted. **Figure 3** shows the storage and loss modulus measured during a strain sweep test. When the storage modulus is higher than the loss modulus, the material shows a solid-like behavior. In the opposite condition, the material shows fluid-like behavior. Except for 0B50R ink, all the other inks have a solid-like behavior at lower strain and a fluid-like behavior at higher strain. As a consequence, the inks will behave like an elastic solid, and they will flow when the strain is high enough. Even though the antisagging additive is not present, 0B55R and 0B60R inks show solid-like behavior, as shown in **Figure 3a**. This effect could be explained by the formation of aggregates due to physical or ionic interactions among the filler particles. Furthermore, hydrogen bonds between the ester groups of the acrylic resin and the silanol groups of the glass fiber surfaces may contribute to the solid-like behavior. Even though the above-mentioned interactions would occur also in 0B50R ink, which is the lower concentration of rGFRP, and consequently of rGF, it could be not enough to induce a solid-like behavior, as shown in **Section 2.2.3**. Considering the second set of inks (**Figure 3b**), the BYK additive contributes to the formation of hydrogen bonds, thanks to the interactions of the amide groups with the ester groups of the acrylic resin and the silanol groups of rGFRPs. By increasing the rheological modifier content, the crossover point shifts toward higher strains, confirming the formation of a more extended hydrogen-bonding structure.

2.2.3. Solid-Like Behavior Recovery

The recovery time of the solid-like behavior after extrusion is a key parameter for the self-standing ability of the inks. Therefore, a too long recovery time will cause a collapse of the deposited ink. As shown in **Figure 4**, a three-step strain test was designed to simulate the ink 3D printing process and measure the viscoelastic response during the time. Two oscillation strains before (0.01%) and after (20%) the crossover point were identified (**Figure 3**). More in detail, the first step of the test simulates the material deformation occurring in the syringe reservoir

(0.01% strain), whereas the second and the third step simulate the ink deformation during the extrusion (20% strain) and after the deposition (0.01% strain), respectively. These steps are shown in **Figure 4a**.

By increasing the filler content from 50 to 60 wt%, the recovery time of the solid-like behavior in the third step decreases from thousands to tens of seconds (**Figure 4b**). A remarkable result is instead achieved by adding 6 or 9 wt% of BYK additive. As shown in **Figure 4c**, 6B55R and 9B55R inks show a rapid transition from liquid-like to solid-like behavior in the third step of the test.

The so far presented rheological analysis proved the inks' extrudability by comparing the experimental curves with the analytical model. Furthermore, the addition of an antisagging agent reduced the viscosity alteration during material handling and during the time. In addition, the BYK additive induced a rapid fluid-like-to-solid-like transition, which is a key property to foster the self-standing ability of 3D-printable inks.

2.3. 3D Printing Process

Compared with FDM, the DIW process with highly viscous inks has a lower control over the material extrusion. Rapid flow rate changes are difficult to achieve as sudden flow stops. In the literature, rheological modification of the inks was presented as a solution not only to enhance the extrusion control but also to introduce the ability to stop the material extrusion when needed.^[18,29,30] As demonstrated by rheological analysis, the rGFRP filler when mixed with the acrylic resin showed a small, yet important, intrinsic ability to exhibit solid-like behavior (**Figure 4a**). Moreover, the addition of a rheological modifier improved the transition between fluid-like and solid-like behaviors (**Figure 4b**).

To further study the recycled composite inks, the influence of the BYK additive content over the 3D printing process was studied by conducting three different tests. The first one, called the flow test, was useful to identify the presence of a flow stabilization time and compare the theoretical and experimental flow rates. The second test, called the residual extrusion test, was conducted to measure the residual extrusion, which was defined as the material leakage after the stop of the extrusion. The third test,

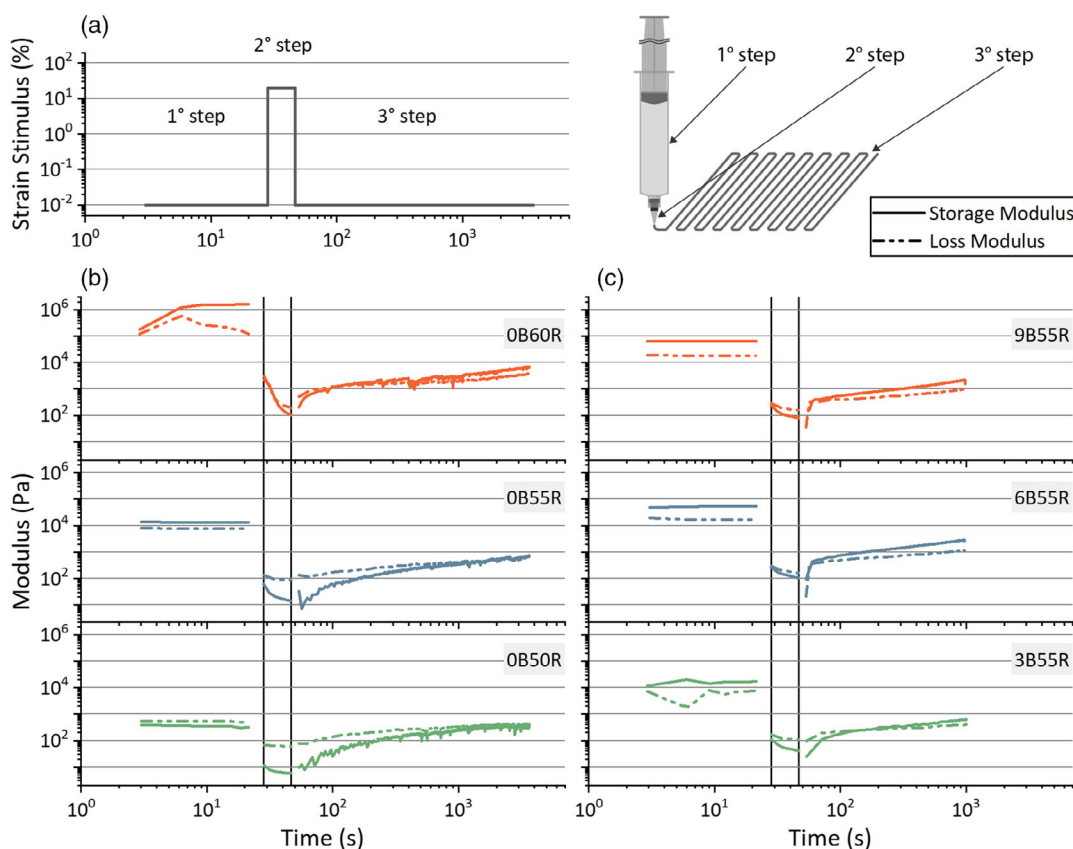


Figure 4. Three-step strain tests. a) Strain applied in the three steps as a function of time. Log–log plots of the storage and loss modulus as a function of time during the application of the strain stimulus in the three steps. b) Inks without the rheological modifier and different wt% of recylate. c) Inks with different wt% of the rheological modifier and 55 wt% of the recylate.

named the retraction stability test, was finally conducted to evaluate the extrusion stability during the repeated flow stops (retractions) and restarts.

2.3.1. Flow Test

As shown in **Table 2**, only 9B55R ink was successfully extruded at the three flow rates studied. During the test at 2.4 and 4.8 mm³ s^{−1} flow rate, 3B55R and 6B55R inks stopped flowing from the dispensing tip (Figure S7, Supporting Information). Clogging due to the filler particle accumulation in the tip was observed in the aforementioned tests. This evidence suggests that the filler has time to aggregate and concentrate in the exit zone at a lower flow rate, preventing a continuous extrusion. Literature also shows that fibers, contained in a polymeric ink, can stick to the internal surface of the tip, progressively obstructing the flow path.^[31] A higher content of the antisagging agent helped prevent filler aggregation in 9B55R ink. This could be due to a higher concentration of groups forming hydrogen bonds, thanks to the presence of the rheological modifier, which hindered the formation of filler particle interactions.

Overall, the flow test evidenced that the experimental flow measured after stabilization time is in good accordance with the theoretical flow rate. Moreover, the stabilization time appears to not have a dependence on the flow rate or the rheological

modifier content. An average time of 230 s is needed to develop a stable material flow rate.

2.3.2. Residual Extrusion Test

Residual extrusion tests were useful for the estimation of the retraction amount needed to stop the material flow. After the stabilization of the ink flow, the piston of the syringe was suddenly

Table 2. Results of the flow test: theoretical flow rate, average experimental flow rate, and average stabilization time.

Ink	Th. flow rate [mm ³ s ^{−1}]	Exp. flow rate [mm ³ s ^{−1}]	Stabilization time [s]
3B55R	2.4	n.a.	n.a.
	4.8	n.a.	n.a.
	9.7	9.7 ± 0.4	218 ± 62
6B55R	2.4	n.a.	n.a.
	4.8	n.a.	n.a.
	9.7	9.0 ± 1.3	249 ± 64
9B55R	2.4	2.4 ± 0.1	199 ± 16
	4.8	4.7 ± 0.2	259 ± 23
	9.7	9.5 ± 0.8	191 ± 30

Table 3. Residual extrusion and required retraction evaluated through the residual tests.

Ink	Residual extrusion [mm ³]	Calculated retraction [mm]
3B55R	342 ± 85	1.2 ± 0.3
6B55R	257 ± 159	0.9 ± 0.5
9B55R	357 ± 70	1.2 ± 0.2

stopped, and the material leakage was weighed to measure the residual extrusion. To compare the results over the three inks, the tests were conducted at a higher flow rate. This represented the condition at which all three formulations were successfully extruded. Even though a trend in the residual extrusion was expected, the results shown in **Table 3** show high variability; thus, a tendency was not highlighted. The theoretical extrusion length was then calculated by dividing the residual extrusion volume by the syringe piston cross section. This ratio was considered as the retraction length needed to stop ink extrusion. Considering that the theoretical retraction average for the three inks is very close to 1 mm, a retraction length of 1 mm was used to test the retraction for all the inks for a matter of simplicity.

2.3.3. Retraction Stability Test

Figure 5 shows the results of the retraction stability test conducted at a flow rate equal to $9.7 \text{ mm}^3 \text{ s}^{-1}$ and a retraction of 1 mm. **Figure 5** shows good stability of the material throughput during the retraction repetition and the material flow is consistent with that measured during the flow tests. **Figure 5** also shows the influence of the BYK additive, confirming the rheological analysis results shown before (**Figure 4c**). As a matter of fact, the ink containing 3 wt% of the antisagging agent showed a serious leakage after the last retraction. In contrast, 9B55R inks, which showed similar rheological behavior to 6B55R ink, exhibited the lowest leakage amount over the three inks. From the information gathered with the three experiments discussed earlier, 9B55R ink was selected as the ink with an optimal BYK concentration, considering good printability over a wide range of

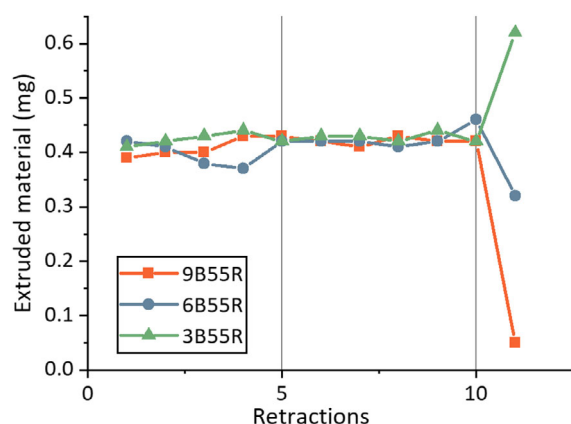


Figure 5. Weight of ink extruded for 30 s at a volumetric flow of $9.7 \text{ mm}^3 \text{ s}^{-1}$ after each retraction. After the last retraction, the extruder was stopped, and the weight of the leaked ink was reported in the graph.

flow rates and the negligible material leakage after syringe piston retraction.

2.3.4. Components Manufacturing

To test the optimized ink, different 3D objects were manufactured. The layer height was fixed at 0.35 mm and the printing velocity at 15 mm s^{-1} , corresponding to a constant flow rate of $5.25 \text{ mm}^3 \text{ s}^{-1}$. To test the retraction, this feature was essential for the 3D printing of all the structures because they required the movement of the extrusion head among the different parts of the objects without leaking material during the nonprinting routes. **Figure 6** shows the 3D models and the corresponding manufactured objects: an extrusion head support (**Figure 6a,b**) and a preassembled chain (**Figure 6c,d**). The manufacturing of the extrusion head support, shown in Video S1, Supporting Information, took more than 4 h to finish and during the process, three 20 mL syringes were changed by pausing the print. As visible in the video, the object showed no plate adhesion problems with the glass plate. Moreover, the extrusion head support produced by DIW showed good dimensional accuracy, and no deformations occurred after the object removal from the build plate. As discussed in Section 2.3.5, the mechanical properties of the 3D-printed 9B55R ink are suitable for this application. Consequently, these achievements allowed the aforementioned extrusion head support to substitute the counterpart manufactured with FDM technology (Video S1, Supporting Information).

Figure 6d shows the 3D-printed chain. As shown, it is composed of three parts designed to rotate against each other. The chain is preassembled, and a clearance of 0.8 mm was left between the rotating joints. The printed chain shows not only the dimensional accuracy of the whole process but also demonstrates the successful use of the retraction mode. Thanks to this feature, commonly used in the FDM process, no leakage of material from the dispensing tip was observed during the movement between one part of the object to the other. Consequently, the three components of the preassembled chain were kept disjointed from each other, allowing them to rotate freely, as shown in Video S2, Supporting Information.

2.3.5. Tensile Tests

A batch of 3D-printed specimens composed of 9B55R ink was also produced. The experimental values of the tensile tests are shown in **Table 4**. These results were then compared with the tensile properties of a conventional material for FDM 3D printing.^[32–34] In detail, polyethylene terephthalate glycol-modified (PETG) was chosen as a reference, as the technical component proposed as a proof of concept (the extrusion head support is shown in **Figure 6**) was originally manufactured with this specific material. As shown in **Table 4**, the developed material shows higher rigidity compared with the PETG. In contrast, its tensile strength is lower. Despite its brittle behavior, the developed material seems to be suitable for the manufacturing of the selected piece. As a matter of fact, the main function of the extrusion head support is to sustain the components of the extruder and the syringe. This piece would be not subjected to excessive deformations, and the increased rigidity related to the material

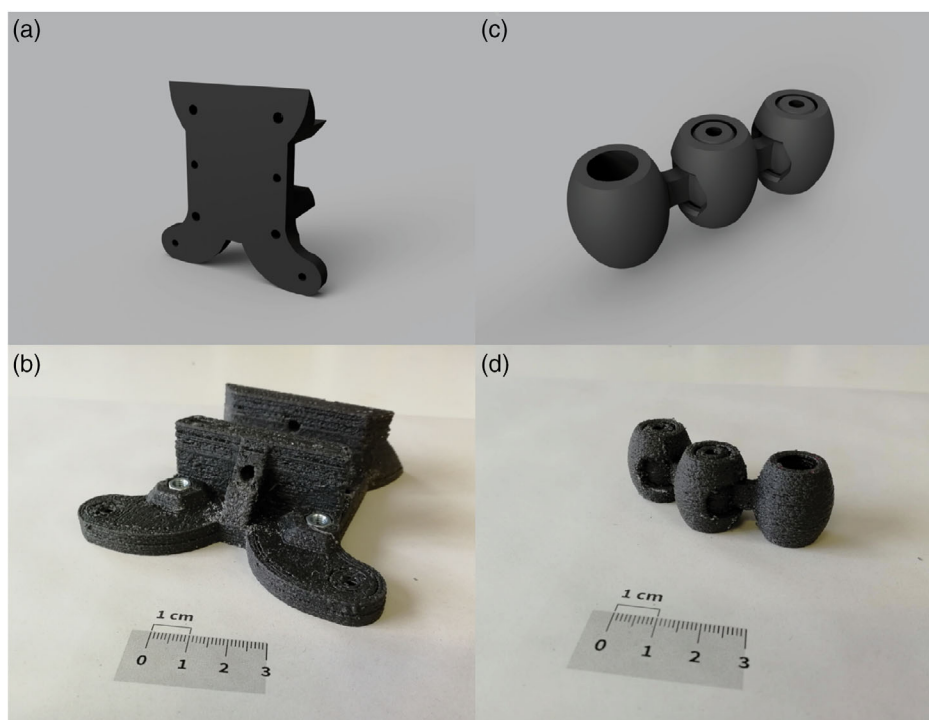


Figure 6. 3D models and 3D-printed structures. Print head support: a) 3D model and c) manufactured object. Preassembled chain: b) 3D model and d) manufactured object.

Table 4. Comparison of the mechanical properties of 9B55R specimens from UV-assisted DIW and PETG specimens from FDM (elastic modulus and tensile strength).

Material	Elastic modulus [GPa]	Tensile strength [MPa]
9B55R	4.5 ± 0.6	20.9 ± 3.0
PETG ^[32–34]	1.6 ± 2.0	31 ± 52

allows the vibration reduction of the extruder during 3D printing, improving the overall accuracy of the final pieces. Moreover, 3D-printed 9B55R samples loaded with 55 wt% of rGF exhibit values of tensile strength that are comparable with those measured for 3D-printed samples loaded with virgin glass fibers (26.3 ± 1.7 MPa),^[26] confirming the opportunity of replacing virgin glass fibers with rGFRPs with the benefit of recycling wasted wind energy blades.

3. Conclusion

The 3D printing process of mechanically recycled composites by UV-assisted DIW was investigated and optimized. The strategy reported in this work enabled a good control of printability for inks composed of an acrylate resin reinforced with shredded EoL GFRP wind blades. Three different percentages of an anti-sagging agent were added to modify the rheological behavior of the inks and better control the DIW process. The addition of the anti-sagging agent in the recycled composite printable inks

enhanced the fluid-like and solid-like transition of the viscoelastic behavior during the extrusion process. A rapid recovery (a few seconds) of the solid-like behavior was observed for composite inks with a higher concentration of rheological modifiers. This indicates the possibility of achieving better shape retention and fidelity for the 3D-printed objects. Specifically, designed printing tests were used to select the optimal content of the anti-sagging agent, enabling the use of the retraction mode for the DIW process. The ink containing 9 wt% of rheological modifiers showed the best performances both for the flow stability over a wide range of flow rates and for the retraction mode. A batch of 3D-printed tensile specimens made with the optimized ink was then tested, and the results confirmed its potential use for the production of structural parts. Complex 3D structures (i.e., a component of the 3D printer and a preassembled structure) were manufactured with the acrylate resin-reinforced rGFRP ink via the UV-assisted DIW process using the retraction for nonprinting movements. The optimization of the ink formulation and the specific 3D printing DIW process promote the reuse of rGF polymer composites in AM technologies to create 3D stiff and high-complexity structures. The rheological tests conducted in this work, i.e., flow ramp, oscillatory, and three-step strain tests, can be essential for the development of other 3D-printable inks to evaluate their extrudability, self-standing ability, and recovery of solid-like behavior after the extrusion. Furthermore, the newly designed printing tests, i.e., flow stabilization, residual extrusion, and retraction stability tests, can play a crucial role in identifying the optimal printing parameters and ink formulations for the DIW process of any materials. Particularly, the parameters

developed in this work for the retraction mode of the DIW process and only used so far for the FDM process can enlarge the number of 3D-printable shapes and structures. These tests can be therefore considered as key guidelines for the development of novel inks in future studies regarding the DIW process.

4. Experimental Section

Material Preparation: 3D-printable inks were obtained by mixing an acrylic-base matrix with rGFRP powders with a Brabender mixer (C.W. Brabender Instruments, Inc, US) equipped with a roller blade (20 min at 40 rpm). The acrylic-base matrix consisted of an ethoxylate bisphenol A diacrylate resin purchased from Arkema and locally distributed by Came S.r.l., Italy. Before obtaining the 3D-printable inks, other components were added to the matrix and mixed with a magnetic stirrer at room temperature for 2 h: the antisagging agent BYK-7411 ES; a solution of a urea-modified agent in amide ester (Sigma-Aldrich, Italy); a thermal activator named dicumyl peroxide (Sigma-Aldrich, Italy); and a photoactivator named ethyl phenyl(2,4,6-trimethylbenzoyl) phosphinate with a commercial name TPO-L (Lambson Limited, UK). Different BYK percentages were investigated during the experimentation, whereas TPO-L and dicumyl peroxide were added using fixed proportions (3 wt% of TPO-L and 0.3 wt% of dicumyl peroxide).

rGFRP powder was obtained by grinding Siemens Gamesa Renewable Energy S.A. EoL wind turbines, which were composed of an epoxy resin reinforced by GF fabric. They were shredded from Consiglio Nazionale di Ricerca—Sistemi e Tecnologie Industriali Intelligenti per il Manifatturiero Avanzato (Stiima-CNR), Italy. The nominal granulometry of the rGFRP powder was 80 μm , the rGF content was 70 wt%, and the average length and diameter of the rGF were, respectively, 34 and 14 μm .^[21] Virgin glass fibers, with the commercial name FIL100, had a nominal diameter of 13 and 100 μm nominal length (Italdry, Italy).

Rheological Measurements: Rheological tests were conducted with Discovery HR-2 (TA Instruments, Inc, US) with a 20 mm plate–plate geometry and 1 mm gap. Except where differently noted, a pre-shear step was applied before the measurements consisting of 10 s^{-1} shear rates for 30 s followed by a 3 min rest period. Afterward, three different tests were performed: a) a stress ramp test from 0 to 20 000 Pa with a linear ramp of 400 Pa min^{-1} ; b) a strain sweep test at 1 Hz from 0.001% to 1000% oscillation strain (forerun by only 3 min rest period); and c) a 3-step oscillation strain test at 1 Hz (forerun by only 3 min rest period), 0.01% strain for 20 s, 20% strain for 20 s and 0.01% strain for 1 h.

3D Printing Tests: Three tests were conducted manually by a Gcode file. Please refer to Note N3, Supporting Information, for a detailed description.

Flow tests: The flow stabilization time and the experimental flow rate were measured by weighing the extruded ink at intervals of 30 s at volumetric flow rates equal to 2.4, 4.8, and 9.7 $\text{mm}^3 \text{s}^{-1}$ (Figure S4, Supporting Information).

Residual extrusion tests: After stabilization time, the syringe piston was stopped, and the residual extrusion due to residual pressure inside the syringe was measured, evaluating the retraction distance needed to stop the ink flow (Figure S5, Supporting Information).

Retraction stability tests: The stability of the extruded ink during the 3D printing process with the retraction mode enabled was tested by repeating the retraction sequence and measuring the weight of the material extruded for 30 s after each retraction (Figure S6, Supporting Information).

The theoretical volumetric flow rate was easily calculated knowing the syringe dimensions and the piston velocity. To compare the volumetric flow rate with the weighed material extrusions, the specific gravity of ink was measured. A beaker was weighed and 20 mL of ink were inserted. The weight of the beaker with the ink was then measured, and the difference was used to calculate the specific gravity, which was 1.4 g cm^{-3} for 0.3-6-9B55R inks.

A commercial 3D printer was modified by specifically designing an extrusion head shown in Figure S1, Supporting Information, and

modifying its firmware.^[27,35,36] The 3D printer was equipped with commercial disposable 20 mL syringes with a Luer Lock and with a UV source, with light emission at 395 nm. For the manufacturing of the tensile samples and the 3D structures, the dispensing tip MT18-PBN was used, whereas TT18-DHUV-PK and TE718025PK (Techon, UK) were also considered for the maximum consistency index (*k*) evaluation.

The tensile properties of the optimized ink (9B55R) after 3D printing were tested to evaluate the feasibility of the proposed applications and components. The tests were conducted by means of a Zwick Roell Z010 (ZwickRoell GmbH & Co. KG, Ulm, Germany) equipped with a 10 kN cell load at a speed of 1 mm min^{-1} , following the ASTM standard test method D3039/D3039M-17.^[37] A batch of five specimens was 3D printed at 15 mm s^{-1} with a layer height of 0.35 mm and a nozzle diameter of 1 mm (flow rate of 5.25 $\text{mm}^3 \text{s}^{-1}$). The nominal gauge length of the specimen was set to 40 mm, whereas the overall dimensions were 10 mm of width, 100 mm of length, and 2 mm of thickness. The major asperities related to 3D printing were removed by manual polishing to achieve a constant cross section for the tensile tests, and the final measures were obtained.

The 3D models of the extrusion head support and the pre-assembled chain were designed with Fusion 360 CAD software (Autodesk, US) and successively processed with Prusa Slicer software (Prusa Research, Czech Republic). The 3D objects were treated with a UV post-curing cycle performed with Polymer 500 W UV chamber (Helios Italquartz S.r.l., Italy) equipped with a UVA emittance mercury vapor lamp type Zs (950 W m^{-2}), for 15 min each side. Afterward, samples were heated in an oven for 2 h at 140 °C, as thermal post-curing treatment. A thermal post-curing treatment was actually needed to increase the polymerization conversion of the 3D printed rGFRP inks, as also previously shown by Romani et al.^[38] The 3D printed materials in fact showed a residual exothermic enthalpy after the UV post-curing and so they were only partially photo-crosslinked. For this reason, a thermal initiator was added to the resin and a thermal post-curing was performed.

Supporting Information

Supporting Information is available from the Wiley Online Library or from the author.

Acknowledgements

This research was funded by European Union's Horizon 2020 research and innovation program for the FiberEUse project: Large Scale Demonstration of New Circular Economy Value-chains based on the Reuse of End-of-life reinforced Composites (project's grant agreement no. 730323). The authors would like to acknowledge Siemens Gamesa Renewable Energy S.A. and Consiglio Nazionale di Ricerca—Sistemi e Tecnologie Industriali Intelligenti per il Manifatturiero Avanzato (Stiima-CNR) for kindly supplying the recycled material.

Conflict of Interest

The authors declare no conflict of interest.

Data Availability Statement

Publicly available datasets were analyzed in this study. The data can be found here: [https://github.com/piuLAB-official/Dataset_A.Mantelli_2021_AEM] (accessed on 22 April 2021). If you will use the data, please cite them in the following way: [dataset] Andrea Mantelli, Alessia Romani, Raffaella Suriano, Stefano Turri and Marinella Levi; 2021; Direct Ink Writing of Recycled COMposites with Complex Shapes: Process Parameters and Ink Optimization; https://github.com/piuLAB-official/Dataset_A.Mantelli_2021_AEM (accessed on 22 April 2021).

Keywords

additive manufacturing, fiber-reinforced plastics, modeling, rheology, 3D printing

Received: January 29, 2021

Revised: April 12, 2021

Published online: May 2, 2021

- [1] Y. Yang, X. Song, X. Li, Z. Chen, C. Zhou, Q. Zhou, Y. Chen, *Adv. Mater.* **2018**, *30*, 1706539.
- [2] Z. Jiang, B. Diggle, M. L. Tan, J. Viktorova, C. W. Bennett, L. A. Connal, *Adv. Sci.* **2020**, *7*, 2001379.
- [3] M. H. Ali, S. Batai, D. Sarbassov, *Rapid Prototyp. J.* **2019**, *25*, 1108.
- [4] Y. Wang, Y. Zhou, L. Lin, J. Corker, M. Fan, *Composites, Part A* **2020**, *139*, 106114.
- [5] P. K. Penumakala, J. Santo, A. Thomas, *Composites, Part B* **2020**, *201*, 108336.
- [6] R. Brighenti, M. P. Cosma, L. Marsavina, A. Spagnoli, M. Terzano, *J. Mater. Sci.* **2021**, *56*, 961.
- [7] T. V. Neumann, M. D. Dickey, *Adv. Mater. Technol.* **2020**, *5*, 2000070.
- [8] Y. Dong, S. Wang, Y. Ke, L. Ding, X. Zeng, S. Magdassi, Y. Long, *Adv. Mater. Technol.* **2020**, *5*, 2000034.
- [9] J. Li, C. Wu, P. K. Chu, M. Gelinsky, *Mater. Sci. Eng.: R* **2020**, *140*, 100543.
- [10] N. W. Solís Pinargote, A. Smirnov, N. Peretyagin, A. Seleznev, P. Peretyagin, *Nanomaterials* **2020**, *10*, 1300.
- [11] K. Chizari, M. A. Daoud, A. R. Ravindran, D. Therriault, *Small* **2016**, *12*, 6076.
- [12] J. Wong, A. T. Gong, P. A. Defnet, L. Meabe, B. Beauchamp, R. M. Sweet, H. Sardon, C. L. Cobb, A. Nelson, *Adv. Mater. Technol.* **2019**, *4*, 1900452.
- [13] B. M. Rauzan, A. Z. Nelson, S. E. Lehman, R. H. Ewoldt, R. G. Nuzzo, *Adv. Funct. Mater.* **2018**, *28*, 1707032.
- [14] A. M'Barki, L. Bocquet, A. Stevenson, *Sci. Rep.* **2017**, *7*, 6017.
- [15] B. Nan, P. Gołębiewski, R. Buczyński, F. J. Galindo-Rosales, J. M. F. Ferreira, *Materials* **2020**, *13*, 1636.
- [16] B. Zhu, J. Pan, B. Nematollahi, Z. Zhou, Y. Zhang, J. Sanjayan, *Mater. Des.* **2019**, *181*, 108088.
- [17] A. V. Rahul, M. Santhanam, H. Meena, Z. Ghani, *Cem. Concr. Compos.* **2019**, *97*, 13.
- [18] H. Sun, Y. Kim, Y. C. Kim, I. K. Park, J. Suhr, D. Byun, H. R. Choi, K. Kuk, O. H. Baek, Y. K. Jung, H. J. Choi, K. J. Kim, J. D. Nam, *J. Mater. Chem. C* **2018**, *6*, 2996.
- [19] X. Tian, T. Liu, Q. Wang, A. Dilmurat, D. Li, G. Ziegmann, *J. Cleaner Prod.* **2017**, *142*, 1609.
- [20] X. Xiao, V. S. Chevali, P. Song, D. He, H. Wang, *Compos. Sci. Technol.* **2019**, *184*, 107887.
- [21] A. Romani, A. Mantelli, R. Suriano, M. Levi, S. Turri, *Materials* **2020**, *13*, 3545.
- [22] C. Hu, L. Hahn, M. Yang, A. Altmann, P. Stahlhut, J. Groll, R. Luxenhofer, *J. Mater. Sci.* **2021**, *56*, 691.
- [23] Y. Ju, J. Ha, Y. Song, J. S. Yun, D. Lee, *Ceram. Int.* **2020**, *46*, 26903.
- [24] T. Beran, T. Mulholland, F. Henning, N. Rudolph, T. A. Osswald, *Addit. Manuf.* **2018**, *23*, 206.
- [25] K. P. M. Lee, M. Brandt, R. Shanks, F. Daver, *Polymers* **2020**, *12*, 2014.
- [26] A. Mantelli, M. Levi, S. Turri, R. Suriano, *Rapid Prototyp. J.* **2019**, *26*, 981.
- [27] A. Mantelli, *Zenodo* **2020**, <http://doi.org/10.5281/zenodo.4283444>.
- [28] *Rheology: Principles, Measurements, and Applications* (Ed: C. W. Macosko), Wiley-VCH, New York **1994**.
- [29] J. A. Lewis, *Adv. Funct. Mater.* **2006**, *16*, 2193.
- [30] B. G. Compton, J. A. Lewis, *Adv. Mater.* **2014**, *26*, 5930.
- [31] B. P. Croom, A. Abbott, J. W. Kemp, L. Rueschhoff, L. Smieska, A. Woll, S. Stoupin, H. Koerner, *Addit. Manuf.* **2020**, *37*, 101701.
- [32] G. Dolzyk, S. Jung, *J. Fail. Anal. Preven.* **2019**, *19*, 511.
- [33] A. Afshar, D. Mihut, *J. Mater. Sci. Technol.* **2020**, *53*, 185.
- [34] S. Petersmann, M. Spoerk, W. Van De Steene, M. Üçal, J. Wiener, G. Pinter, F. Arbeiter, *J. Mech. Behav. Biomed. Mater.* **2020**, *104*, 103611.
- [35] A. Mantelli, *Zenodo* **2020**, <http://doi.org/10.5281/zenodo.4282564>.
- [36] A. Mantelli, *Zenodo* **2020**, <http://doi.org/10.5281/zenodo.4298907>.
- [37] ASTM D3039, **2017**.
- [38] A. Romani, A. Mantelli, M. Levi, in *Proc. of the 19th European Roundtable for Sustainable Consumption and Production – Circular Europe for Sustainability: Design, Production and Consumption*, **2019**, *Book of Papers*, p. 491.